Study of the dynamic formation of transmission gratings recorded in photopolymers and holographic polymer-dispersed liquid crystals

Sébastien Massenot, Jean-Luc Kaiser, Raymond Chevallier, and Yvon Renotte

Local and nonlocal models for the diffusion of photopolymers are applied to the dynamic formation of transmission gratings recorded in photopolymers and holographic polymer-dispersed liquid crystals (H-PDLCs). We retrieve the main parameters of H-PDLCs (refractive-index modulation and diffusion coefficient) by combining a solution of the one-dimensional diffusion equation and the rigorous coupled-wave theory applied to transmission gratings. The rigorous coupled-wave theory method provides us with information on higher harmonics of the refractive profile (not only on the first harmonic as when the classical Kogelnik theory is applied). Measurements concerning the second harmonic validate the modeling.

1. Introduction

Holographic optical elements are taking a more important place in telecommunications and information processing. Functions such as switching, spectrum analysis or equalization, data storage, and filtering can be realized with diffractive elements fabricated holographically. For this to be extended to an industrialization phase, we need holographic materials that are low cost and easy to use. Photopolymers are a serious candidate for meeting these requirements. They are self-processing materials, and the development is dry, unlike dichromated gelatin, which requires a specific chemical process.

Photopolymers have been widely studied and several models have been developed, as in Refs. 1–3. In particular, it has been shown that the diffusion process is nonlinear with the exposure energy and that harmonics appear.[4] The idea proposed here is to validate a diffusion model for photopolymers by use of the experimental values of the second-order grating. This phase will help us to validate the method used in the present paper.

Holographic polymer-dispersed liquid crystals (H-PDLCs) are known to be a promising technology. They can find applications in telecommunications (dynamic spectral equalization[5]) and information processing by providing switchable holograms, data storage, and color reflective displays. H-PDLCs can range from simple gratings to two-dimensional and three-dimensional structures as photonic crystals.[6]

H-PDLCs are attractive materials as they have the advantages of photopolymers cited previously, and the presence of liquid crystals (LCs) provides them with a switchable behavior. During the exposure to an interference pattern [see Fig. 1(a)], a phase separation occurs between the monomer and the LC droplets owing to the diffusion process. Polymerization occurs in bright regions, the monomer diffuses from dark to bright regions, and the LC diffuses in the opposite direction. So, after the exposure, the H-PDLC system consists of alternating layers of polymer planes and LC-rich droplet planes as shown on Fig. 1(b).

By use of a monomer whose polymer's refractive index is equal to n_o (ordinary index of the LC), the recorded structure can be erased by applying a voltage (all the LC molecules are aligned along the ordinary axis). Hence their possible application to photonic switching, which is one of the key functions in reconfigurable optical networks.

For such applications, we need to know precisely

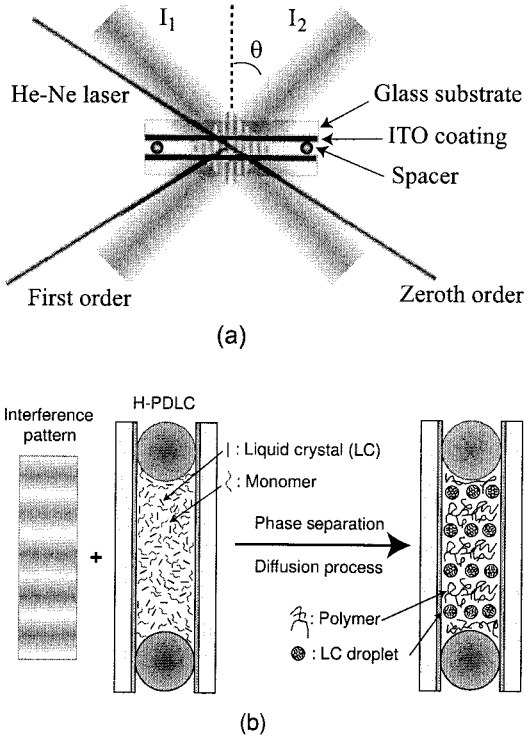

Fig. 1. (a) Classical experimental setup used for recording transmission holographic gratings in photopolymers or H-PDLCs and (b) illustration of the diffusion process when a H-PDLC cell is illuminated with an interference pattern. ITO, indium tin oxide.

the values of the parameters of the material used. For photopolymers and H-PDLCs, it is possible to determine and control these parameters by studying the dynamic formation of holograms. Some pertinent information concerning the refractive-index profile can be derived from a diffusion model. In our case, we are more interested in these materials from a diffractive point of view, and we retain as pertinent information the values of the first and second harmonics of the refractive profile.

The fact that we do not need a chemical process for the development of the holograms allows us to study in real time the formation of the grating by using an attenuated He–Ne laser and by recording the diffracted powers in the zeroth and first orders as shown on Fig. 1(a).

By monitoring the grating formation process and by combining a diffusion model for the photopolymerization and a diffraction modeling algorithm, we shall be able to make some preliminary conclusions concerning the refractive-index profile of the grating and its temporal evolution and to retrieve an estimate of the diffusion coefficient of the monomer. Then it will be easier to optimize the recording process and to obtain reproducible components, which is a key of future industrialization.

In the first part we shall present the theoretical aspects of the diffusion process for photopolymers and H-PDLCs. The numerical methods used for the diffusion equations and diffraction efficiency calculation and the way that we will get the values of the main parameters of these two materials, such as the diffusion coefficient or the refractive-index modulation, will be given. Then experimental and fitted results will be presented for photopolymers and H-PDLCs.

2. Theoretical Aspects

A. Diffusion Model

1. *Local Model*

Our analysis uses a classical model of diffusion that has been developed for photopolymers.[1] In this paper we are interested in the diffusion of one kind of monomer. Because the diffusion constant of LC is larger than for monomers,[7] we can assume that the LC redistribution is given by the mass conservation law.

The diffusion equation for the concentration of monomers is given by

$$\frac{\partial \phi(x, t)}{\partial t} = \frac{\partial}{\partial x}\left[D(x, t) \frac{\partial \phi(x, t)}{\partial x} \right] - F(x, t)\phi(x, t), \tag{1}$$

with $\phi(x, 0) = \phi_0$, where $\phi(x, t)$ is the monomer concentration, $D(x, t)$ is the diffusion coefficient, and $F(x, t)$ is the polymerization rate. The first term of the right-hand side of this equation corresponds to the diffusion of free monomers, and the second term represents the photopolymerization process. The expressions of the diffusion coefficient and the polymerization rate are given by

$$D(x, t) = D_0 \exp[-\alpha F(x, t)t], \tag{2}$$

with α as the diffusion coefficient decay parameter, and

$$F(x, t) = \kappa\{I_0[1 + V \cos(Kx)]\}^{1/2}, \tag{3}$$

where $I_0 = I_1 + I_2$ is the exposure energy (I_1 and I_2 are related to the two beams interfering), $V = 2\sqrt{I_1 I_2}/(I_1 + I_2)$ is the fringes' visibility, $K = 2\pi/\Lambda$ (Λ is the period of the recorded grating) is the modulus of the grating vector, and κ is the polymerization rate coefficient. The product Kx corresponds to the one-dimensional scalar product $\mathbf{K} \cdot \mathbf{r}$.

We can also write the equation for the concentration of the polymer:

$$\frac{\partial \Psi(x, t)}{\partial t} = F(x, t)\phi(x, t), \tag{4}$$

with $\Psi(x, 0) = 0$, where $\Psi(x, t)$ is the polymer concentration.

In photopolymers the refractive index is linked to the density of polymers. Concerning the index profile, we assume that $n(x, t) = c_n[\phi(x, t) + \Psi(x, t)]$, where c_n is a proportionality constant that links the monomer (or polymer) concentration to its index

value. So we can write a differential equation for the evolution of the refractive-index profile:

$$\frac{\partial n(x, t)}{\partial t} = c_n \frac{\partial}{\partial x}\left[D(x, t)\frac{\partial \phi(x, t)}{\partial x}\right], \tag{5}$$

with $n(x, 0) = n_0$.

At the end of the recording process, the refractive-index profile is not sinusoidal, and it can be written as a Fourier series expansion:

$$n(x) = n_0 + \sum_{i=1}^{+\infty} n_i \cos\left(\frac{2i\pi x}{\Lambda}\right). \tag{6}$$

This can be interpreted as a superposition of gratings with periods Λ/i with respective index modulations n_i. n_1 will refer to the primary grating (purely sinusoidal) and n_2 to the secondary grating.

2. Nonlocal Model

In the previous model it is assumed that the polymerization process is a local one and that the effect at a certain point is independent of other places. It has been shown that disagreements occur between predictions of this model and experimental results for high-spatial-frequency gratings.[2] It means that polymer chains can grow away from their starting point, which leads to a spreading of the polymer and a more sinusoidal index profile.[8]

The diffusion equations can be rewritten under the form

$$\frac{\partial \phi(x, t)}{\partial t} = \frac{\partial}{\partial x}\left[D(x, t)\frac{\partial \phi(x, t)}{\partial x}\right] - \int_{-\infty}^{+\infty} G(x, x')F(x', t)\phi(x', t)\mathrm{d}x', \tag{7}$$

$$\frac{\partial \Psi(x, t)}{\partial t} = \int_{-\infty}^{+\infty} G(x, x')F(x', t)\phi(x', t)\mathrm{d}x', \tag{8}$$

with

$$G(x, x') = \frac{1}{\sqrt{2\pi\sigma}}\exp\left[\frac{-(x - x')^2}{2\sigma}\right]$$

as the nonlocal response function, where σ is the polymer chain-length variance growing away from the initiation point. This distribution will have the effect of spreading the polymer concentration.

B. Solving of the Diffusion Equations

The problem that we have to solve is classified in the parabolic equations with periodic boundary conditions. We will use a finite-difference scheme to solve this set of equations. The numerical method retained is the Crank–Nicholson method, which is known to be automatically stable whatever the time step and more accurate than the classical explicit and implicit methods (see, for example, Ref. 9). The Crank–Nicholson method evaluates partial derivatives at the instant $t + \frac{1}{2}$ by calculation of the mean of the explicit and implicit methods. By attribution of the indexes i, j to the variables x and t on the solving mesh, the finite-difference scheme for the monomer equation is given by Eq. (9):

$$\begin{aligned}\frac{\phi_i^{j+1} - \phi_i{}^j}{\Delta t} = \frac{1}{2}\Bigg(&\frac{D_{i+1}^{j+1} - D_{i-1}^{j+1}}{2\Delta x}\frac{\phi_{i+1}^{j+1} - \phi_{i-1}^{j+1}}{2\Delta x} \\ &+ D_i^{j+1}\frac{\phi_{i+1}^{j+1} - 2\phi_i^{j+1} + \phi_{i-1}^{j+1}}{\Delta x^2} - F_i^{j+1}\phi_i^{j+1}\Bigg) \\ &+ \frac{1}{2}\Bigg(\frac{D_{i+1}^{j} - D_{i-1}^{j}}{2\Delta x}\frac{\phi_{i+1}^{j} - \phi_{i-1}^{j}}{2\Delta x} \\ &+ D_i{}^j\frac{\phi_{i+1}^{j} - 2\phi_i{}^j + \phi_{i-1}^{j}}{\Delta x^2} - F_i{}^j\phi_i{}^j\Bigg),\end{aligned} \tag{9}$$

with the periodic boundary conditions $\phi_0{}^j = \phi_N{}^j$ and $\phi_{-1}^j = \phi_{N-1}^j$.

This equation can be written in a matrix form, which is easier to compute and faster than using an iterative method at each time step:

$$(\mathbf{I} - \mathbf{M}^{j+1})\phi^{j+1} = (\mathbf{I} - \mathbf{M}^j)\phi^j, \tag{10}$$

where $\mathbf{I}$ is the identity matrix and $\mathbf{M}$ is an $N \times N$ matrix of the form

$$\mathbf{M} = \frac{\Delta t}{2}\{[\partial x]\mathbf{D}[\partial x] + [\mathbf{D}][\partial x^2] - [\mathbf{F}]\}. \tag{11}$$

Matrices $[\partial x]$ and $[\partial x^2]$ correspond to operators representing the first- and second-derivative operations by use of a finite-difference scheme. $[\mathbf{D}]$ and $[\mathbf{F}]$ are diagonal matrices with elements D_i and F_i, and $\mathbf{D}$ is a column vector with elements D_i. Taking into account the periodic boundary conditions, we find that the first- and second-derivative operators are of the form

$$[\partial x] = \frac{1}{2\Delta x}\begin{bmatrix} 0 & 1 & 0 & \dots & -1 \\ -1 & 0 & 1 & & 0 \\ 0 & \ddots & \ddots & \ddots & \vdots \\ \vdots & & -1 & 0 & 1 \\ 1 & \dots & 0 & -1 & 0 \end{bmatrix},$$

$$[\partial x^2] = \frac{1}{\Delta x^2}\begin{bmatrix} -2 & 1 & 0 & \dots & 1 \\ 1 & -2 & 1 & & 0 \\ 0 & \ddots & \ddots & \ddots & \vdots \\ \vdots & & 1 & -2 & 1 \\ 1 & \dots & 0 & 1 & -2 \end{bmatrix}. \tag{12}$$

So, one can easily obtain ϕ^{j+1} by inverting the matrix $\mathbf{I} - \mathbf{M}^{j+1}$ by a standard algorithm such as lower-triangular–upper-triangular factorization.[9] For the refractive-index profile, we apply the same method. Then, by applying a fast Fourier transform to the refractive-index profile, we can obtain the temporal evolution of the different harmonics (we will be mainly interested in the first and second harmonics).

In the case of the nonlocal model the integral is calculated with a trapezoidal rule:

$$\int_{-\infty}^{+\infty} G(x, x')F(x', t)\phi(x', t)\mathrm{d}x' \simeq \frac{dx}{2}\left[v(1, j) + 2\sum_{k=2}^{N-1} v(k, j) + v(N, j)\right], \quad (13)$$

with $v(k, j) = G(x_i, x_k)F(x_k)\phi(x_k, j)$. The matrix [**F**] has to be replaced in Eq. 11.

C. Transmission Gratings Modeling

The standard Kogelnik's theory[10] for thick gratings may become inaccurate especially when the Q factor of the grating is lower than 10, when we are far from the Bragg condition, or when the grating is too dispersive and it can become strongly polarization dependent. In addition, it is well known that the refractive-index profile for gratings recorded in photopolymers is not purely sinusoidal and that harmonics of higher order can appear, which is not predicted or directly calculated by Kogelnik's theory. For these reasons, we use a rigorous modeling tool: the rigorous coupled-wave theory.[11] In our case, the stable implementation was used[12] in order to avoid contaminations due to positive and real exponential terms to prevent numerical instabilities.

D. Determination of the Diffusion Parameters

By monitoring the recording process with a He–Ne laser, we record the temporal evolution of the zeroth and first diffracted orders, and we retrieve the evolution of the refractive-index modulation (or the first-harmonic coefficient of the polymer concentration) by using the rigorous coupled-wave theory. We obtain a function $n_1^{\exp}(t)$.

Then, following Ref. 8, we use a quasi-Newton method requiring lower- and upper-boundary values for the unknown parameters. At each function call, the diffusion equation is solved, and the first-harmonic evolution $n_1(D_0, \kappa, \alpha, c_n, t)$ is obtained. We calculate the error between the experimental data and the calculations:

$$\mathrm{Error}(t) = \overline{|n_1(D_0, \kappa, \alpha, c_n, t) - n_1{}^{\exp}(t)|}. \quad (14)$$

We search to minimize this error function with a constraint on the second-harmonic value, which has to be lower than the measurement. At the beginning of the optimization process, it is better to start with quite realistic initial values to avoid local minima.

One can check the validity of the fitting of the parameters by the agreement of numerical results with the monitoring curves by comparing them with typical values found in the literature and by inserting the refractive-index profile obtained with the optimization process directly into the rigorous coupled-wave theory rather than a classical sinusoidal profile. The calculated profile will agree if it closely fits the angular characterization when the first and second diffracted orders are taken into account. The model that we are going to keep will be one that will give us the more reasonable values for the physical parameters.

3. Experiments

A. Experimental Setup

The experimental setup is presented on Fig. 1(a): It is a standard two-plane-wave interference setup. We prepare a H-PDLC cell by inserting a preparation monomer–LC between two glass substrates coated with indium tin oxide. A photoinitiator (Rose Bengal dye in our case) is added to the preparation to activate the reaction of polymerization. The laser used for the recording is an Ar^+ at 514.5 nm. The period of the recorded grating is given by $\Lambda = \lambda/(2 \sin \theta)$ (relation in the air). The He–Ne laser used in this case is TE polarized (parallel to the fringes of the grating). In the following, we will work only with this polarization state. After the recording we do a UV postexposition to polymerize all the remaining monomer.

B. Recordings on DuPont Photopolymers

1. Experimental Results

We first did holographic recordings in DuPont Omnidex HRT-700-20 photopolymers (see Acknowledgments) to validate our method by comparing the fitting results to classical values found in the literature. We recorded gratings with a period of 0.882 μm (chosen sufficiently dispersive to separate correctly the diffracted beams of the Ar^+ and He–Ne lasers). This period has been determined by the measurement of diffraction angles and refined with rigorous coupled-wave analysis (RCWA). In these experiments the cell was not presented as on Fig. 1(a) but with a photopolymer film deposited on a glass substrate. The sample is exposed on the glass substrate side to avoid a decrease of the fringes' visibility because of the birefringence of the Mylar film recovering the material.

To determine the parameters of the model, we realized four recordings at different exposure energies. The recording process has been stopped at the steady state. Using the rigorous coupled-wave theory, we obtain the following curves for the temporal evolution of the refractive-index modulation. Results are presented on Figs. 2(a) and 2(b).

The diffraction efficiencies that are plotted on Fig. 2(a) are relative efficiencies (in that case, losses due to Fresnel reflections are automatically taken into account). For such a grating, which is quite dispersive, we can assume that we have only the zeroth and first diffracted orders at Bragg incidence. The two curves on Fig. 2(a) that have a maximum before the steady state indicate that the gratings are overmodulated (the refractive-index modulation is higher than the modulation required to give a maximum diffraction efficiency in the first order at Bragg incidence).

We angularly characterize the gratings, and we

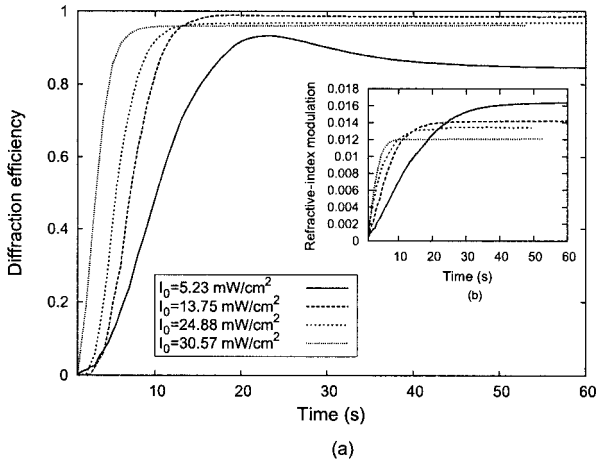

Fig. 2. (a) Temporal evolutions of diffraction efficiency and (b) corresponding refractive-index modulation for gratings recorded in DuPont photopolymers at four exposures.

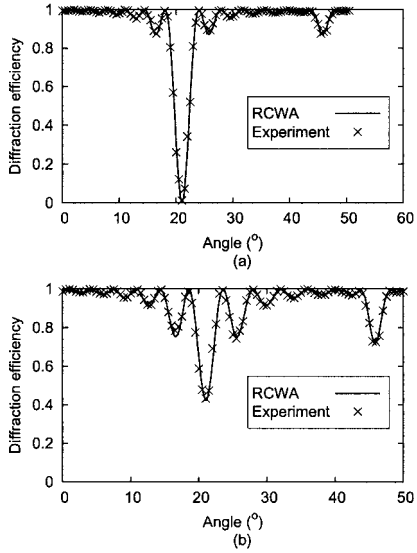

Fig. 3. Angular evolutions of the diffraction efficiency for two gratings recorded in DuPont photopolymers with exposures of (a) 30 mW/cm^2 and (b) 3.7 mW/cm^2.

retrieve the main parameters by using the rigorous coupled-wave theory.

The values of the refractive-index modulations are given in Table 1, where n_1 and n_2 are, respectively, the index modulations of the first and secondary gratings [see Eq. (6)] and T is the thickness of the grating. These values differ a little with the monitoring curves when they are at steady state; this can be due to the fact that the He–Ne laser is not precisely at Bragg incidence (the angular response is quite narrow) and due to the UV postexposition, which increases the index modulation. We do not take into account eventual shrinkage effects of the photopolymer film during the UV exposure.

We now present on Figs. 3(a) and 3(b) the angular measurements' results and compare them with the theory given by the rigorous coupled-wave theory for two gratings when different exposure energies are considered.

The accordance between measurements and RCWA is quite good. The angular response of the grating in Fig. 3(b) is due to overmodulation.

2. *Optimization Results*

To simplify the problem, we will assume that the diffusion coefficient is constant ($\alpha = 0$). We take $\phi_0 = 100$ mol/cm^3 (typical value) as the initial value for the monomer concentration. The parameter κ can be approximated directly from the experimental results, and it has been shown that the steady state is reached for a value of the normalized time $t_D = \kappa\sqrt{I_0}\, t_{\text{steady}} = 10$. This leads to an optimization problem of only two or three parameters in the nonlocal model case. Knowing the value of κ, we will not use directly the diffusion coefficient D_0 but rather a dimensionless parameter called R_D, which avoids manipulation of very small numbers for the optimization (D_0 is of the order of 10^{-11}). The expression of R_D is given by

$$R_D = \frac{D_0 4\pi^2}{\kappa\sqrt{I_0}\,\Lambda^2}. \tag{15}$$

We tried two algorithms, one using the constraint on the second harmonic and the other unconstrained. The results obtained by the optimization process are given in Table 2.

We note that, for the unconstrained algorithm, refractive-index modulations are overevaluated, hence the need to check the value of the second harmonic calculated by the model. If we keep only the constrained algorithm for the nonlocal model, we obtain the values given in Table 3.

We can see that the constraints of optimization are respected for both models (values for n_1 and n_2) but that the results for the diffusion coefficients are different by a factor of 10 or more. Concerning the nonlocal model, if we plot the diffusion coefficient as a function of the exposure energy, we obtain an exponential curve [see Fig. 4(a)]. Hence we can write $D(I_0) = D_0 \exp(\beta I_0)$. Using a standard curve-fitting routine, we get

$$D(I_0) = 1.80 \times 10^{-11} \exp(0.0689 I_0). \tag{16}$$

We apply the same process to c_n: It appears to be roughly linear versus I_0; we obtain

$$c_n(I_0) = 4.92 \times 10^{-6} I_0 + 5.24 \times 10^{-4} \tag{17}$$

[see Fig. 4(b)].

Table 1. Grating Parameters Recorded in Photopolymers Determined with the Rigorous Coupled-Wave Analysis

Grating	Exposure I_0 (mW/cm^2)	T (μm)	n_1	n_2
1	5.23	22.5	0.0172	0.0035
2	13.75	22.5	0.0155	0.0039
3	24.75	22.5	0.0145	0.0032
4	30.57	23	0.0138	0.0031

Table 2. Fitting Results Obtained with the Local Model Applied to Photopolymers

Grating	Algorithm	R_D	D_0 (10^{-11} cm^2/s)	c_n (10^{-4} cm^3/mol)	κ [(cm/$\sqrt{\text{mW}}$)/s]	n_1	n_2
1	unconstrained	2.9018	8.2251	2.6653	0.0629	0.0164	0.00507
	constraint	10.5848	30.1239	2.3299	0.0629	0.0164	0.00354
2	unconstrained	1.7821	9.6207	2.8659	0.0739	0.0142	0.00609
	constraint	6.2578	45.6572	2.3526	0.0739	0.0142	0.00385
3	unconstrained	1.2152	12.9134	2.9984	0.1084	0.0134	0.00693
	constraint	11.9133	97.5631	2.1186	0.1084	0.0134	0.00318
4	unconstrained	1.64014	29.3753	2.4933	0.1644	0.0121	0.00539
	constraint	8.0652	144.4498	1.9643	0.1644	0.0121	0.00309

Concerning the nonlocal length σ, it does not seem to depend on the exposure energy: We keep the mean value, giving $\sqrt{\sigma} = 106.29$ nm.

According to the literature,[8,3,13] the order of magnitude of the diffusion coefficient is 10^{-11}, hence there is a best fitting with the nonlocal model. In addition, because the error function was higher with the local model than with the nonlocal model, there are greater difficulties when fitting experimental data with the first model. It is possible to fit correctly experimental data with the local model, but the values predicted for the second harmonic are quite wrong.

3. *Predictions Given by the Model*

We now check the model described above by attempting to fit the monitoring curves of the gratings recorded in photopolymers only by using previously calculated values. We recorded two gratings with exposures $I_0^1 = 13.6$ mW/cm^2 and $I_0^2 = 21.81$ mW/cm^2. The temporal evolution of the first harmonic calculated with the diffusion equations by use of the fitting parameters is inserted in the RCWA program. A comparison between experimental and predicted diffraction efficiencies is given in Fig. 5.

A comparison between values obtained for the first and second harmonics of the refractive-index profile with experimental results are provided in Table 4.

We note that predicted values are in quite good accordance with the corresponding measured values of n_1 and n_2. The values of the parameters obtained by the optimization process can be validated for the exposure range of energy studied. The behaviors of D_0 and c_n may change for quite low exposure energies.

In addition, we have to keep in mind that such results depend strongly on the performance of the values given by the minimization algorithm of a function of several variables (the error function in our case). Such functions can present several local minima, but the constraint on the second-order grating helps the algorithm to avoid some of these local minima.

C. Recording on Holographic Polymer-Dispersed Liquid Crystals

We shall now apply the same study to H-PDLCs. In contrast to DuPont photopolymers, H-PDLC materials are not commercially available, and we have to process them. So a first task is to determine a composition for which we shall get acceptable diffraction efficiencies in the first order (typically more than 70%).

1. *Processing*

First, we tested four different preparations by varying the concentrations of LCs and added another monomer for two preparations. The compositions are related in Table 5. These data are given in percentages of the total weight. The meanings of the abbreviations are

- DPHPA: dipentaerythritol penta- and hexaacrylate (monomer),
- HexF: hexafluoroisopropyl acrylate (monomer),
- VN: vinyl neononanoate (monomer),
- P-I: photoinitiator,
- BL036: liquid crystal.

The component HexF has the property of enhancing the phase separation and reducing switching voltages,[14] and the monomer VN is here in order to have a preparation less viscous. The P-I solution has different components. Its composition is Rose Bengal (2%), N-phenylglycine as a coinitiator (6%), and the

Table 3. Fitting Results Obtained with the Nonlocal Model Applied to Photopolymers

Grating	R_D	D_0 (10^{-11} cm^2/s)	κ [(cm/$\sqrt{\text{mW}}$)/s]	$\sqrt{\sigma}$ (nm)	c_n (10^{-4} cm^3/mol)	n_1	n_2
1	0.9106	2.6288	0.0629	111.93	5.1025	0.01644	0.003549
2	0.8501	4.5896	0.0739	100.98	4.3257	0.01488	0.003861
3	0.8710	9.4477	0.1084	108.46	4.1627	0.01341	0.003184
4	0.8591	15.39	0.1644	103.79	3.7021	0.01205	0.003093

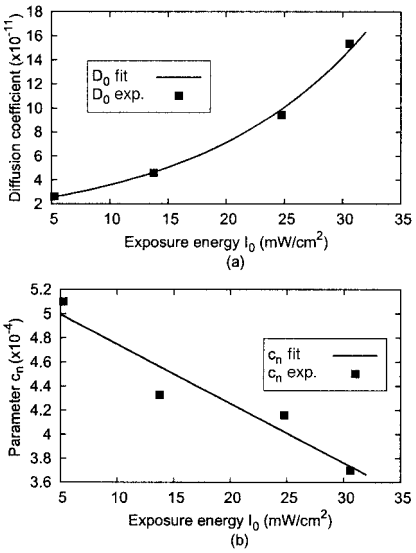

Fig. 4. Evolutions of (a) the diffusion coefficient D_0 and (b) the coefficient c_n according to the exposure energy for photopolymers.

two reactive diluents 1-vinyl-2-pyrrolidinone (46%) and trimethylolpropane tris(3-mercaptopropionate) (46%).

After the recording, the H-PDLC samples undergo a UV postexposition in order to terminate the reaction and to consume the remaining colorant (Rose Bengal). The H-PDLC film becomes nearly transparent after sufficient postexposure.

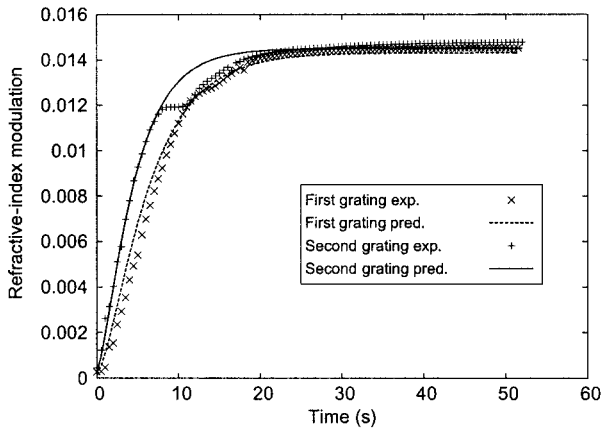

Fig. 5. Comparison between experimental and predicted values of the temporal evolution of the refractive-index modulation for two gratings.

Table 4. Comparison of Experimental and Predicted Values of the Refractive-Index Modulations for Two Gratings Recorded in Photopolymers

Exposure I_0 (mW/cm^2)	n_1^{exp}	n_1^{pred}	n_2^{exp}	n_2^{pred}
13.6	0.01451	0.01435	0.00335	0.00359
21.81	0.01479	0.01451	0.00295	0.00305

Table 5. Composition of the Different H-PDLC Preparations

Preparation	DPHPA	HexF	VN	P-I	BL036
A	49.9	12.1	—	10.2	27.8
B	42.4	12.4	—	10.1	35.1
C	47.5	9.5	5.1	10.1	27.8
D	44.4	10.3	10.2	6	29.1

2. *Comparison of the Preparations*

We plot here the monitoring curves for the first-order diffraction efficiency. The exposure energy was the same for all samples.

In the case of the preparations A and B [Fig. 6(a)], even if the curves have a maximum and a decrease, there are no overmodulation effects as previously for photopolymers. This has been proved by our measuring angular selectivity and fitting with RCWA. The fast-rising peak observed is due to an overexposure of the preparation. In this case, the rate of formation of free radicals is faster than the diffusion rate. It means that most of the monomers are polymerized before the diffusion process, and it results in an inefficient index modulation. It is different for preparations C and D [Fig. 6(b)] in which the evolution is quite smooth. The advantage of adding the monomer VN is shown.

We will select for the following study the preparation D. In that one monomer species (DPHPA) is primarily being used here, we will assume that we will have only one monomer in the diffusion equations.

3. *Dynamic Study for Preparation D*

We made recordings for two different exposures (the two gratings will be called G_1 and G_2; we have $I_0{}^{G_1} = 34.88\ \text{mW/cm}^2$ and $I_0{}^{G_2} = 72.11\ \text{mW/cm}^2$). We kept

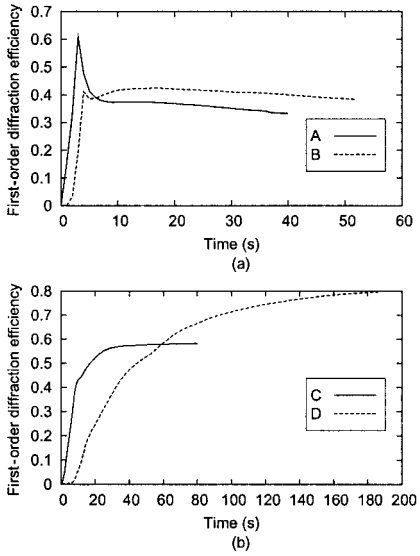

Fig. 6. Temporal evolution of the first-order diffraction efficiency for four different H-PDLC mixtures: (a) A and B and (b) C and D. The composition of each mixture is given in Table 5.

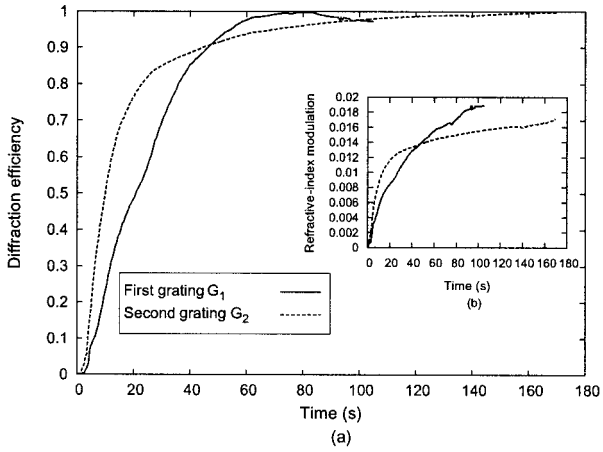

Fig. 7. (a) Temporal evolutions of diffraction efficiency and (b) corresponding refractive-index modulation for the two gratings G_1 and G_2 recorded by use of the H-PDLC mixture D at different exposure energies.

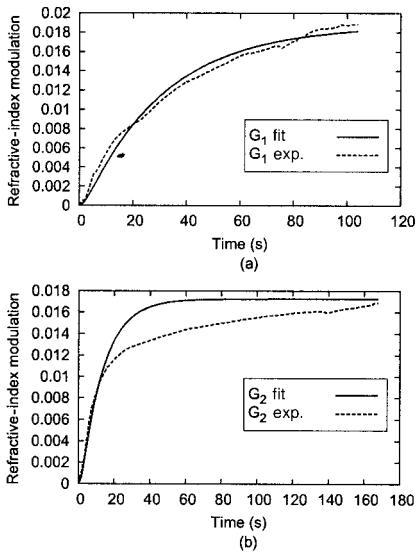

Fig. 8. Temporal evolution of the refractive-index modulation of the two gratings G_1 and G_2: (a) experimental results and (b) values given by the diffusion model.

the previous period of 882 nm. The monitoring curves are given in Figs. 7(a) and 7(b). The index modulation values are given in Table 6.

As for the photopolymers, we measured relative efficiencies; Fresnel losses, material absorption, or scattering losses are not taken into account. Spacers of 18 μm were used for building the cells. An average index modulation of 0.02 is obtained. We note that the second harmonic decreases as a function of the exposure energy to reach values for which the grating is not overmodulated.

4. Fitting Results

As for the results obtained with photopolymers, the nonlocal model will be used. We use a proportion of monomer for the initial value of ϕ_0. The distribution of LC droplets will be evaluated by the mass conservation law. Performing the same process as for photopolymers, we obtain the fitted values of the parameters: $D_0 \simeq 1 \times 10^{-10}$ cm^2/s, $c_n = 5.09 \times 10^{-4}$ cm^3/mol, and $\sqrt{\sigma} \simeq 80$ nm. We can see the fitting results on Figs. 8(a) and 8(b). We can remark that, for the first exposure, fitting and experimental data are in quite good accordance, but there are some differences for the second exposure. The first parts of the curves are correctly fitted, but differences occur after. We explain this behavior by the fact that we have several monomers in the H-PDLC solution of H-PDLC and the one monomer model is no longer applicable under a high exposure. The diffusion equations have to be solved with several monomers with different diffusion constants.

Table 6. Parameters of the Two Gratings Recorded in H-PDLC

Grating	Exposure I_0 (mW/cm^2)	n_1	n_2
1	34.88	0.021	0.0061
2	72.11	0.019	0.0049

4. Conclusion

We have studied the dynamic formation of transmission gratings in classical photopolymers and in the promising material of H-PDLCs.

Subsection 3.B helped us to validate the diffusion model and to choose the optimization method, given the fact that these materials have been studied deeply. The proposed model could be improved by use of two coefficients for the refractive-index profile (one for the monomer and one for the polymer) or taking into account the time decay of the diffusion polymerization rate.

By comparing experiments and results predicted by the theory, it appears that it is important to know the values of the parameters of the secondary grating (photopolymers or H-PDLCs) to obtain accurate values with the fitting procedure. Such multivariable functions may have several local minima, which can lead to wrong results. Taking into account an additional constraint on the second harmonic increases the probability of obtaining correct values.

We compared the characteristics of different preparations and retained the one that gave us the best diffraction efficiency in the first order. More than 90% relative diffraction efficiency has been measured. The monitoring allows us to check the behavior of the photopolymerization process and to avoid too-fast-rising peaks that lead to weak index modulations. The model for H-PDLCs is not as accurate as for photopolymers. We obtained approximate values that help us to predict the global behavior of the recording process. The simple two-component model presented here should be considerably improved. First, the presence of several monomers (with different viscosities) should be taken into account and, then, effects such as the anisotropic diffusion of LCs if we want to approach the real refractive-

index profile. It will lead to an increase of the number of equations and of the parameters to find during the optimization process. Powerful routines such as genetic algorithms may have to be used.

The authors acknowledge Yvon Renotte from the laboratory "Hololab" of the Liège University for hosting the experiments concerning photopolymers. J. L. Kaiser acknowledges Gregory P. Crawford for useful discussions on the technology of the H-PDLC.

References

1. G. Zhao and P. Mouroulis, "Diffusion model of hologram formation in dry photopolymer materials," J. Mod. Opt. **41,** 1929–1939 (1994).
2. J. T. Sheridan and J. R. Lawrence, "Nonlocal-response diffusion model of holographic recording in photopolymer," J. Opt. Soc. Am. A **17,** 1108–1114 (2000).
3. V. Moreau, Y. Renotte, and Y. Lion, "Characterization of DuPont photopolymer: determination of kinetic parameters in a diffusion model," Appl. Opt. **41,** 3427–3435 (2002).
4. G. Zhao and P. Mouroulis, "Second order grating formation in dry holographic photopolymers," Opt. Commun. **115,** 528–532 (1995).
5. J. L. Kaiser, G. P. Crawford, R. Chevallier, and J. L. de Bougrenet de la Tocnaye, "Chirped switchable reflection grating in holographic PDLC for wavelength management and processing in optical communication systems," Appl. Opt. (to be published).
6. M. J. Escuti, J. Qi, and G. P. Crawford, "Tunable face-centered-cubic photonic crystal formed in holographic polymer dispersed liquid crystals," Opt. Lett. **28,** 522–524 (2003).
7. C. C. Bowley and G. P. Crawford, "Diffusion kinetics of formation of holographic polymer-dispersed liquid crystal display materials," Appl. Phys. Lett. **76,** 2235–2237 (2000).
8. S.-D. Wu and E. Glytsis, "Holographic grating formation in photopolymers: analysis and experimental results based on a nonlocal diffusion model and rigorous coupled-wave analysis," J. Opt. Soc. Am. B **20,** 1177–1188 (2003).
9. W. H. Press, S. A. Teutolsky, and W. T. Vetterling, *Numerical Recipes in C: The Art of Scientific Computing*, 2nd ed. (Cambridge U. Press, Cambridge, UK, 1992).
10. H. Kogelnik, "Coupled wave theory for thick hologram gratings," Bell Syst. Tech. J. **48,** 2909–2947 (1969).
11. M. G. Moharam and T. K. Gaylord, "Three-dimensional vector coupled-wave analysis of planar grating diffraction," J. Opt. Soc. Am. A **73,** 1105–1112 (1983).
12. M. G. Moharam, E. B. Grann, D. A. Pommet, and T. K. Gaylord, "Formulation for stable and efficient implementation of the rigorous coupled-wave analysis of binary gratings," J. Opt. Soc. Am. A **12,** 1068–1076 (1995).
13. F. T. O'Neill, J. R. Lawrence, and J. T. Sheridan, "Comparison of holographic photopolymer materials by use of analytic nonlocal diffusion models," Appl. Opt. **41,** 845–852 (2002).
14. M. De Sarkar, J. Qi, and G. P. Crawford, "Influence of partial matrix fluorination on morphology and performance of HPDLC transmission gratings," Polymer **43,** 7335–7344 (2002).